Synthesis, Crystal Structure, EPR, and DFT Studies of an Unusually Distorted Vanadium(II) Complex

Philip Charles,[a,b] Mallory E. Gaspard,[a,b] Santiago Alvarez,[c] Micah S. Ziegler,[d] Amgalanbaatar Baldansuren,[a,b] William H. Armstrong,[e] K. V. Lakshmi,[a,b,*] and Peter J. Bonitatibus Jr.[a,*]

SUPPLEMENTARY INFORMATION

Table of contents:

1- Materials

All manipulations were performed under an atmosphere of purified N_2 or Ar (grade 4.8) using standard Schlenk or dry box techniques. Chemicals were obtained from commercial sources, but never used without further purification (unless indicated otherwise). Solvents were doubly distilled under Ar from the specified drying agents and degassed prior to use through three successive freeze-pump-thaw cycles: THF, first Na/K alloy then $LiAlH_4$; diethyl ether, Na ribbon then $LiAlH_4$; pentane, distilled once from Na ribbon; dimethoxyethane (DME), distilled once from $LiAlH_4$. Triflic acid (CF_3SO_3H), *n*-BuLi (1.6 M in hexanes), and VCl_3 were used as received. The compounds $[VCl_3(THF)_3]$, $V(CF_3SO_3)_3$, and $[V(THF)_4(CF_3SO_3)_2]$ were prepared by published procedures [1,2]. The racemic ligand 3,3'-di-*tert*-butyl-5,5',6,6'-tetramethyl-1,1'-biphenyl-2,2'-diol (H_2TBDMPD) was prepared by a published procedure developed by Schrock and coworkers, [3] however is commercially available from Sigma Aldrich. Zinc dust (used to prepare $[V(THF)_4(CF_3SO_3)_2]$) and solid H_2TBDMPD were each heated separately and evacuated for 2 days at 120°C. Elemental analyses was performed by Robertson Microlit Laboratories, Inc., 29 Samson Ave., P.O. Box 927, Madison, NJ, 07940. Infrared spectra were taken on a Nicolet 210 FT-IR spectrophotometer using NaCl plates.

2- Dilithiation of 3,3'-di-tert-butyl-5,5',6,6'-tetramethyl-1,1'-biphenyl-2,2'-diol

Racemic diol, H_2TBDMPD, (1.51 g, 4.24 mmol) was dissolved in 35 mL of pentane. *n*-BuLi (5.56 mL of a 1.6 M solution in hexanes) was added dropwise over 10 minutes at room temperature and deprotonation proceeded overnight. The homogeneous

solution was pumped to dryness and the resulting light beige powdered material could be used without further purification in reactions with $[V(THF)_4(CF_3SO_3)_2]$.

Racemic diol, H_2TBDMPD: 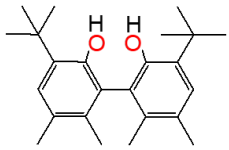

3- Synthesis of $[V(TBDMPD)_2\{Li(DME)\}_2]$ complex

To a mixture of $[V(THF)_4(CF_3SO_3)_2]$ (0.2 g, 0.31 mmol) and Li_2TBDMPD (0.23 g, 0.63 mmol) were added 10 mL of THF in a 20 mL reaction vial. The reaction changed color slowly from sky blue to a light brown homogeneous solution after 45 minutes and was left to stir overnight. Pumping to dryness gave microcrystalline green-brown flakes. The compound was extracted with a small amount (3-5 mL) of Et_2O to deposit $Li(CF_3SO_3)$ (too much Et_2O solubilizes $Li(CF_3SO_3)$), filtered, and pumped to dryness. $[V(TBDMPD)_2\{Li(THF)\}_2] \cdot 2\ Et_2O$ was obtained as a light brown powder (78% yield). EPR (THF): 4 K, g = 3.7 and 1.9 (sharp 8-line patterns superimposed); Anal.: found (calc'd): C: 66.89(67.68)%, H: 9.01(9.65)%, N: <0.02(0.00)%; IR (nujol mull, NaCl plates, cm^{-1}): 1425(s), 1404(s), 1284(s), 1272(vs), 1175(s), 1049(s), 917(m), 894(m), 873(m), 863(m), 799(m), 682(w), 651(m).

With the addition of a small amount of DME to an Et_2O solution of $[V(TBDMPD)_2\{Li(THF)\}_2] \cdot 2\text{-}Et_2O$, a greenish-brown solution deposited dichroic green-brown blocks of $[V(TBDMPD)_2\{Li(DME)\}_2] \cdot 2\text{-}Et_2O$ by standing at 0^oC overnight.

Reaction Scheme 1:

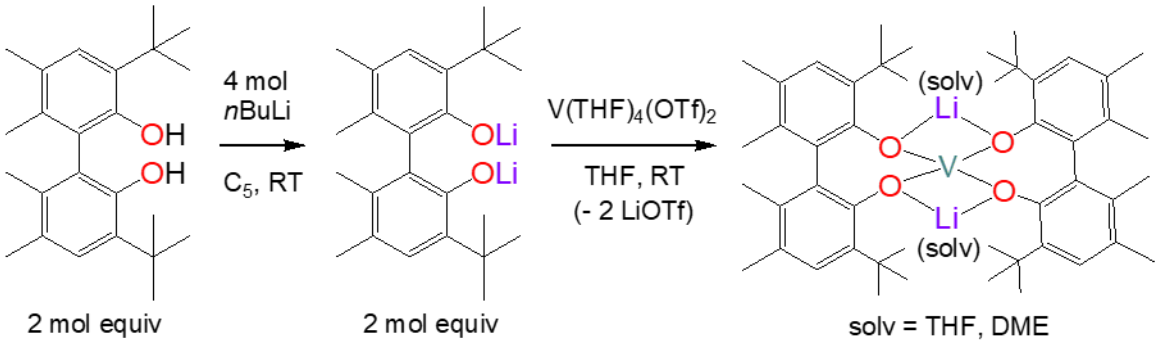

4- Continuous-wave EPR spectroscopy

The EPR spectra of compound **1** and compound **2** were recorded on a Bruker ECS-106 and custom-designed Bruker Elexsys E580 spectrometer, respectively. The spectrometer was equipped with a dual-mode resonator and the temperature was controlled by an Oxford E900 cryostat for liquid helium measurements (9 K). Selected instrumental parameters: microwave frequency at 9.660 GHz; modulation frequency of 100 kHz; modulation amplitude of 4 G; microwave power of approximately 12.6 mW for Compound **1** and 1 – 2 mW for Compound **2**.

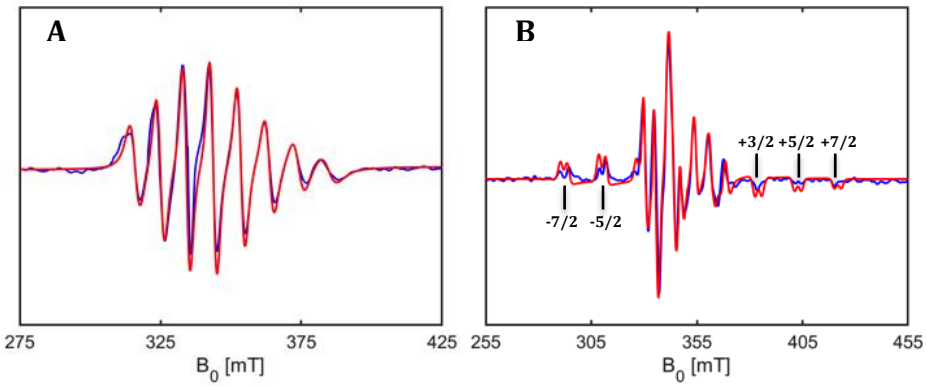

Figure S1. Continuous-wave X-band EPR spectrum of compound **2** using toluene as a solvent at **(A)** room temperature and **(B)** 9 K. The experimental and numerically simulated EPR spectrum are shown as a blue and red trace, respectively. The experimental spectra were obtained at a microwave frequency of

9.66 GHz, modulation frequency of 100 kHz, modulation amplitude of 4 G and microwave power of 1 – 2 mW. The numerical simulations of the experimental spectra yielded a **g**-tensor of [1.978, 1.980, 1.933] and hyperfine **A**-tensors of [174, 156, 499] MHz and [-9.98, 6.24, 80.0] MHz for ^{51}V and ^{13}C, respectively.

5- Spectral simulations

The *cw* EPR spectra of a frozen solution of the ^{51}V complexes, Compound **1** and Compound **2**, in THF and toluene solvent, respectively, were numerically simulated using the "pepper" function of the software package, EasySpin 5.2.25 [4]. The simulated spectra were compared to the experimental spectra to match the positions of the EPR signals, peak separations due to the ^{51}V hyperfine coupling and effects of zero-field splitting on the line shapes. The signal intensity distribution over the different points of the experimental spectra were also reproduced in the spectral simulations. The experimental and simulated spectra were plotted in Matlab 2019b.

6- Density functional theory (DFT) calculations

The density functional theory (DFT) calculations of compound **1**, $[V(TBDMPD)_2\{Li(THF)\}_2]$, were performed with a BHLYP functional [5] and pc-3/ZORA-def2-SVP basis set [6,7] using the software program, ORCA 4.0.1.2 [8]. The initial coordinates for the complex were obtained from the X-ray crystal structure of compound **1** and the model contained a total of 151 atoms. A ZORA-def2-SVP basis set was used for most of the atoms in the model while the pc-3 basis set was incorporated for the $^{51}V^{2+}$ and Li^{+} ions. The RIJCOSX approximation was employed to speed up the calculations [9]. In order to estimate the effect of the exchange functional and basis set,

the electron density distribution and hyperfine parameters that were obtained with the BHLYP functional and pc-3/ZORA-def2-SVP basis were compared with those obtained by using the same basis with a variety of other functionals and basis sets for the $^{51}V^{2+}$ and Li^{+} ions (see below, Supplementary Table S1). We observed that the BHLYP functional with the pc-3/ZORA-def2-SVP basis provided the most accurate hyperfine couplings that were validated by comparison with the analogous hyperfine couplings that were experimentally determined by cryogenic continuous-wave EPR spectroscopy measurements and *vice versa*.

A well-characterized VO^{2+} complex, $VO(Gly)_2$, with a known X-ray crystal structure and EPR parameters was used as model to evaluate the computational methods in this study [7]. The results indicated that a BHLYP functional with an SVP basis set yielded the best agreement with the experimental value of A_{iso} of -275 MHz (Table S2). This is in agreement with previous studies by Larsen and Saladino that had calculated the A_{iso} values were of VO^{2+} complexes using nine different functionals with the software package, Gaussian98, and found that the accuracy of the A_{iso} values successively improved on going from the pure GGA functionals (BLYP, BP86, and BPW91) to the hybrid B3 functionals (B3LYP, B3P86, and B3PW91) to the half-and-half hybrid functionals (BHLYP, BHPW91, and BHP86) [7].

7 - DFT Tables S1 and S2

Supplementary Table S1.
Dependence of the hyperfine tensor (A_X, A_Y, A_Z) and isotropic hyperfine coupling (A_{iso}) on the choice of functional and basis set in the DFT calculations of compound **1** in this study. Highlighted in bold font are the hyperfine parameters that are obtained with a hybrid functional, BHLYP, and pc-3 basis set for the $^{51}V^{II}$ and Li^{I} ions in complex **1**.

Method	^{51}V A_x (MHz)	^{51}V A_y (MHz)	^{51}V A_z (MHz)	^{51}V A_{iso} (MHz)
EPR	**-108.00**	**-55.00**	**-84.00**	**-82.30**

Functional/Basis set	^{51}V A_x (MHz)	^{51}V A_y (MHz)	^{51}V A_z (MHz)	^{51}V A_{iso} (MHz)
B3LYP/ZORA-def2-SVP	36.13	17.37	-43.31	-3.40
B3LYP/6-311g(d,p)	30.65	12.54	-51.17	-2.66
ωB97X/ZORA-def2-SVP	-53.41	27.11	9.18	-5.70
ωB97X-D3/ ZORA-def2-SVP	-58.94	3.37	21.84	-11.24
ωB97X-D3/ ZORA-def2-TZVP	-57.21	5.01	24.05	-9.38
BHLYP/ZORA-def2-SVP	-21.38	-42.26	-100.07	-54.57
BHLYP/def2-SVP	-19.09	-38.66	-99.45	-52.40
BHLYP/ZORA-def2-TZVP	-24.25	-45.79	-103.60	-57.88
BHLYP/def2-QZVP	-51.50	-108.16	-28.28	-62.65
BHLYP/pc-3	**-108.50**	**-28.33**	**-52.33**	**-63.05**
BHLYP/6-311g(d,p)	-21.38	-42.25	-100.07	-54.57
BHANDHLYP/ZORA-def2-SVP	-21.38	-42.26	-100.07	-54.57
BHANDHLYP/def2-SVP	-19.09	-38.66	-99.45	-52.40
B3PW91/ZORA-def2-SVP	18.31	-1.61	-58.43	-13.91
B3PW91/def2-SVP	-12.02	-6.84	-66.27	-20.37
B3PW91/pc-3	17.64	-5.41	-60.48	-16.08

Supplementary Table S2.
Dependence of the hyperfine tensor (A_X, A_Y, A_Z) and isotropic hyperfine coupling (A_{iso}) on the choice of functional and basis set in the DFT calculations of the model, $VO(Gly)_2$. Highlighted in bold font are the hyperfine parameters that are obtained with a hybrid functional, BHLYP, and ZORA-def2-SVP basis set that are in best agreement with the experimental parameters [7].

Functional/Basis set	^{51}V A_x (MHz)	^{51}V A_y (MHz)	^{51}V A_z (MHz)	^{51}V A_{iso} (MHz)
BHLYP/ZORA-def2-SVP	**-179.00**	**-480.84**	**-160.14**	**-273.33**
BHLYP/def2-SVP	-152.92	-457.57	-133.76	-248.08
BHLYP/ZORA-def2-TZVP	-189.25	-496.29	-170.16	-285.23
BHLYP/def2-TZVP	-155.74	-465.71	-136.41	-252.62
BHLYP/def2-TZVPD	-154.79	-464.82	-135.43	-251.68
BHLYP/def2-TZVPP	-158.63	-472.58	-139.56	-256.93
BHLYP/def2-TZVPPD	-158.11	-472.02	-139.02	-256.38
BHLYP/def2-QZVP	-163.66	-482.74	-146.38	-264.26
BHLYP/pc-3	-163.66	-482.74	-146.38	-264.26
B3PW91/def2-SVP	-112.80	-393.62	-90.46	-198.96
B3PW91/def2-TZVP	-114.6	-399.18	-92.29	-202.02
B3PW91/def2-TZVPD	-113.27	-397.92	-90,93	-200.70
B3PW91/def2-TZVPP	-116.64	-404.10	-94.50	-205.08
B3PW91/def2-TZVPPD	-115.43	-402.86	-93.27	-203.85
B3PW91/def2-QZVP	-118.34	-409.60	-97.92	-208.62
B3PW91/pc-3	-116.84	-410.18	-96.85	-207.96

8 – X-ray crystallographic details and Tables S3 for compound 1

X-ray crystallography was performed on a SMART CCD area detector diffractometer using graphite-monochromated MoKα radiation provided by a sealed X-ray tube at 50 kV and 40 mA. Large dichroic green-brown blocks (~0.7 mm^3) were isolated from mother liquor by using a pipette, deposited onto a microscope slide, and covered with deoxygenated heavy mineral oil (Exxon Paratone N). Crystals were manipulated, evaluated, and one selected under a microscope. The specimen was mounted on a thin glass fiber with the aid of a mixture of Paratone oil and high-vacuum silicon grease using a rolled-up Kimwipe®, and transferred immediately to the cold stream (-90 ºC) of the SMART CCD area detector diffractometer. Unit cell parameters were determined using an automatic routine in SMART. [10]

Data collection proceeded by acquisition of 1,270 10 sec. frame images using a scan width of 0.3º from 3.75º to 56.65º in 2θ. A total of 19,280 reflections were collected of which 9,595 were determined to be unique. These frames were then subjected to scanning for, and integration of data by the SAINT program to obtain a set of integrated reflection intensities. [11] Final unit cell parameters were calculated using the full data set.

The resultant data was processed using the SHELXTL-Plus suite of programs. [12] Direct methods routines allowed for solution of the structure. There are two solvate Et_2O molecules. All non-hydrogen atoms were refined using anisotropic thermal parameters, including those of the Et_2O units of solvate. Hydrogen atoms were placed in idealized positions and refined using a riding model. The thermal parameters of the hydrogen atoms were set to 1.3 times one third of the trace of the orthogonalized U-

tensor of the carbon to which they are attached. Full-matrix least squares refinements were computed on F^2 values with residuals calculated according to preset formulas. Additional crystallographic data have been deposited with the Cambridge Crystallographic Data Centre (CCDC).

Supplementary Table S3. Crystal data and structure refinement details for $[V(TBDMPD)_2\{Li(DME)\}_2] \cdot 2Et_2O$.

Empirical formula	$C_{64}H_{104}Li_2O_{10}V_1$
Formula weight	1098.29
Temperature	183(2) K
Wavelength	0.71073 Å
Crystal system	Monoclinic
Space group	C2/c
a	23.733(1) Å
b	11.9979(6) Å
c	22.787(1) Å
$\alpha = \gamma$	90 deg.
β	95.004(1) deg.
Volume, Z	6463.9(5) $Å^3$, 4
Density (calculated)	1.129 g/cm^3
Absorption coefficient	0.206 mm^{-1}
F(000)	2388
Crystal size	0.7 x 0.5 x 0.35 mm
2θ range for data collection	3.44 to 56.62 deg.
Limiting indices	$-31 \le h \le 21$, $-15 \le k \le 15$, $-30 \le l \le 29$
Reflections collected	19273
Independent reflections	8018 [R_{int} = 0.0377]
Data / restraints / parameters	8018 / 42 / 371
Goodness-of-fit on F^2	1.062
Final R indices [$I>2\sigma(I)$]	R_1 = 0.0516, wR_2 = 0.1394
Largest diff. peak and hole	0.85 and -0.41 $e \cdot Å^{-3}$

9 – X-ray crystallographic details and Table S4 for compound 2

Supplementary Table S4. Crystal data and structure refinement details for $[V(TBDMPD)_2]$.

Empirical formula	$C_{48}H_{64}O_4V$
Formula weight	755.93
Temperature	183(2) K
Wavelength	0.71073 Å
Crystal system	Monoclinic
Space group	$P2_1/n$
a	10.1309(4) Å
b	24.5283(9) Å
c	18.0181(7) Å
$\alpha = \gamma$	90 deg.
β	100.636(1) deg.
Volume, Z	4400.5(3) $Å^3$, 4
Density (calculated)	1.141 g/cm^3
Absorption coefficient	0.266 mm^{-1}
F(000)	1628
2θ range for data collection	4.04 to 46.512 deg.
Limiting indices	$-11 \le h \le 10$, $-20 \le k \le 27$, $-20 \le l \le 19$
Reflections collected	18169
Independent reflections	6259 [R(int) = 0.134]
Absorption correction	Semi-empirical from ψ-scans
Max. and min. transmission	0.3466 and 0.2333
Refinement method	Full-matrix least-squares on F^2
Data / restraints / parameters	6259 / 0 / 499
Goodness-of-fit on F^2	1.122
Final R indices [$I>2\sigma(I)$]	R_1 = 0.0895, wR_2 = 0.1481
Largest diff. peak and hole	0.32 and -0.46 $e \cdot Å^{-3}$

10 – Structural references used to generate the shape map (Figure 2)

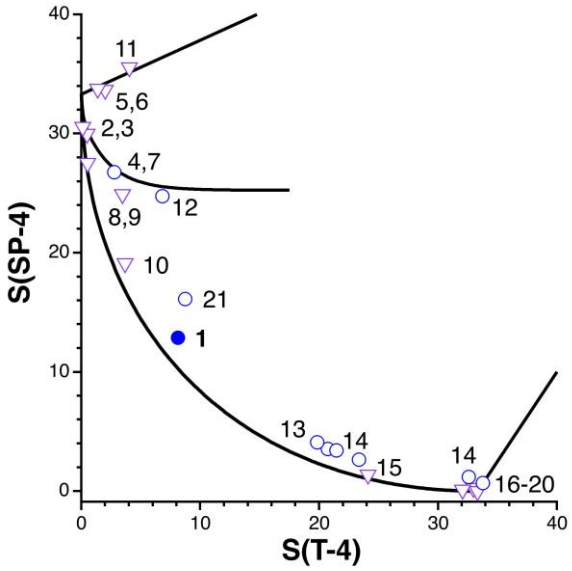

1- Compound **1**	This work.
2- FURTAN, Re(IV)	P. D. Savage, G. Wilkinson, M. Motevalli, M. B. Hursthouse, *J. Chem. Soc., Dalton Trans.*, 1988, 669.
3- JABSOU, Os(V)	J. Arnold, G. Wilkinson, B. Hussain, M. B. Hursthouse, *Chem. Commun.*, 1988, 1349.
4- K_3FeO_4, Fe(V)	R. Hoppe and K. Mader, *Z. Anorg. Allgem. Chem.*, 1990, **586**, 115-124.
5- TOKYIB, Mo(III)	C. E. Laplaza, M. J. A. Johnson, J. C. Peters, A. L. Odom, E. Kim, C. C. Cummins, G. N. George, I. J. Pickering, *J. Am. Chem. Soc.*, 1996, **118**, 8623.
6- VEQGUT, Mo(III)	Y.-C. Tsai, M. J. A. Johnson, D. J. Mindiola, C. C. Cummins, W. T. Klooster, T. F. Koetzle, *J. Am. Chem. Soc.*, 1999, **121**, 10246.
7- PEGDOW, V(II)	B.L. Tran, B. Pinter, A.J. Nichols, F.T. Konopka, R. Thompson, C.-H. Chen, J. Krzystek, A. Ozarowski, J. Telser, M.-H. Baik, K. Meyer, D.J. Mindiola, *J. Am. Chem. Soc.*, 2012, **134**, 13035.
8- JIWRIQ, Cr(III)	P. J. Alonso, L. R. Falvello, J. Forniés, M. A. García-Monforte, A. Martín, B. Menjón, G. Rodríguez, *Chem. Commun.*, 1998, 1721.
9- JIWRIQ01, Cr(III)	P. J. Alonso, J. Forniés, M. A. García-Monforte, A. Martín, B. Menjón, C. Rillo, *Chem. Eur. J.*, 2002, **8**, 4056.
10- LIBCRA, Cr(III)	M. Bochmann, G. Wilkinson, G. B. Young, M. B. Hursthouse, K. M. A. Malik, *J. Chem. Soc., Dalton Trans.*, 1980, 1863.
11- VOCTIQ, Cr(III)	S. Schneider, A. C. Filippou, *Inorg. Chem.*, 2001, **40**, 4674.
12- PERZUH, V(II)	R. K. Minhas, J. J. H. Edema, S. Gambarotta, A. Meetsma, *J. Am. Chem. Soc.*, 1993, **115**, 6710.

13- KELGOX, V(II) M. J. Scott, W. C. A. Wilish, W. H. Armstrong, *J. Am. Chem. Soc.*, 1990, **112**, 2429.
14- IGAXIA, IGAXOG, IGAXUM Y. Sekiguchi, K. Arashiba, H. Tanaka, A. Eizawa, K. Nakajima, K. Yoshizawa, and Y. Nishibayashi, *Angew. Chem*., 2018, **130**, 9202.
15- PITCEA, Cr(III) S. Hao, J.-I. Song, P. Berno, S. Gambarotta, *Organometallics*, 1994, **13**, 1326.
16- SAVKUV10, Re(IV) I. M. Gardiner, M. A. Bruck, P. A. Wexler, D. E. Wigley, *Inorg. Chem.*,1989, **28**, 3688.
17- SAVKUV, Re(IV) I. M. Gardiner, M. A. Bruck, D. E. Wigley, *Inorg. Chem.*, 1989, **28**, 1769.
18- PITCOK, Cr(III) Same reference as PITCEA.
19- NbO, Nb(II) A. L. Bowman, T. C. Wallace, J. L. Yarnell, R. G. Wenzel, *Acta Crystallogr.*, 1966, **21**, 843.
20- PERZOB, V(II) Same reference as PERZUH.
21- GIYDOJ, V(II) A. F. Cozzolino, J. S. Silva, N. López, C. C. Cummins, *Dalton Trans.*, 2014, **43**, 4639.

A closer look at the data for vanadium(II) complexes allows us to conclude that the d^3 electron configuration and the presence of bidentate ligands in **1** and in Cummins's compound (CSD Refcode GIYDOJ) favor a significantly twisted tetrahedral structure.

11 - Shape Analysis of tetracoordinate V compounds in any oxidation state

Here we present a shape map of all tetracoordinate vanadium complexes in oxidation states ranging from +2 to +5, disregarding polyoxometallates, to clearly show how only V(II) compounds have allowed for geometries along the spread distortion path from tetrahedral to square planar geometry.

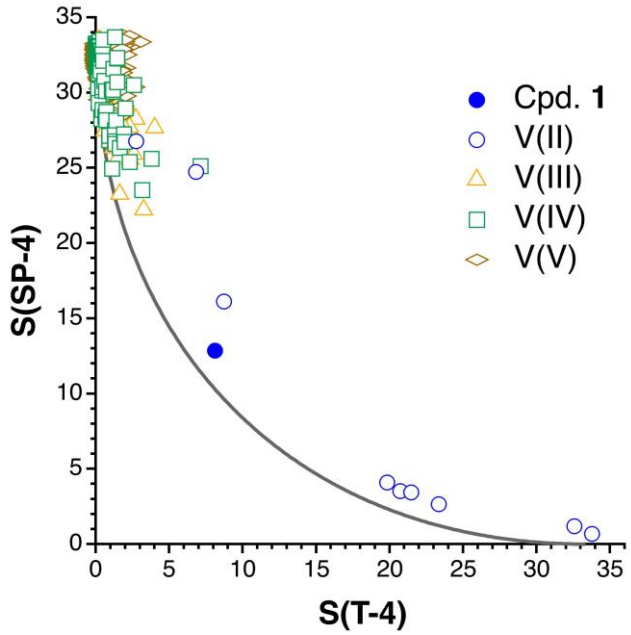

Figure S2. Shape map of tetracoordinate vanadium complexes in oxidation states ranging from +2 to +5; the continuous line represents the spread distortion pathway.

Table S5. Shape analysis of four-coordinate vanadium complexes. Shape measures, degree of distortion and deviation from the minimal distortion path that takes the tetrahedron (T-4) to a planar square (SP-4). In boldface, the shape measure and/or path deviation parameter that best describes the stereochemistry of each compound. Refcodes correspond to CSD database identifiers.

Compound	Ox. state	n[a]	S(T4)	S(SP4)	Dev.[b]	Dist.[b]	Refcode	reference
$[V(OC_6H_4{}^iPr_2)_4]^-$	+3	0	**0.01**	32.97	0.6	1.3	SABLAI	1
$[V(SiPh_3)_4]^-$	+4	0	**0.02**	32.88	1.3	2.1	VAZSUK	2
$[V(O^tBu)_3(OSi\{O^tBu\}_3)]$	+4	0	**0.09**	31.62	1.8	4.8	XIYCIR	3
$[V(O^tBu)_2(OSi\{O^tBu_3\})_2]$	+4	0	**0.14**	31.53	3.1	6.2	XIYCOX	3
$[V(OSi^tBu_3)_3(OP^tBu_3)]$	+4	0	**0.17**	33.44	6.8	6.6	ILOGUL	4
$[V(OSi^tBu_3)_3(OPMe_3)]$	+4	0	**0.43**	32.13	8.8	10.7	ILOGOF	4
$[V(S_2FeCl_2)_2]^{3-}$	+3	2	**2.40**	24.94	10.3	25.3	CEHNOS	5
$[V(N\{SiMe_3\}_2)_2(N\{SiCH_2Me_2\})^-$	+3	1	**2.26**	27.47	14.2	24.5	ROBSEG-V1	6
	+3	1	**2.31**	27.69	14.8	24.8	ROBSEG-V2	6
$[V((O^tBu)_4(Li\{thf\}_2)\{Li(N\{SiMe_3\}_2)\}]$	+3	2	3.54	26.07	17.8	30.8	ROJTIW	7
$[V(Me_2Si\{N^tBu\}_2)_2]$	+4	2	4.69	25.27	20.7	35.1	DUXMEO	8
$[V(PhB\{N^tBu\}_2)_2]$	+4	2	7.13	25.12	29.2	43.9	AJENUY	9
$[V(nacnac)(OAr_2)]$ [c]	+2	1	**2.76**	26.77	15.5	27.1	PEGDOW	10
$[VMe_4]^{2-}$	+2	0	6.33	13.13	**1.6**	**41.3**	Calculated	11
$[V(tmen)(2,6\text{-}OC_6H_3Ph_2)_2]$ [d]	+2	1	6.82	24.75	27.5	42.9	PERZUH	12
Compound **1**	+2	2	8.13	12.86	**6.6**	**47.0**		this work
$[V(5\text{-}MeC_6H_3\{N^tBu\}\{NMe_2\})_2]$	+2	2	8.72	16.13	15.8	48.7	GIYDOJ	13
$[V(OC_6H_4{}^iPr_2)_4]^{2-}$	+2	0	20.72	3.53	**7.5**	76.8	KELGOX	14
$[V(py)_2(3\text{-}Me,2,6\text{-}{}^tBuC_6H_2O)_2]$	+2	0	33.78	**0.68**	**14.1**	**100.8**	PERZOB	12
$[V(PNP)_2(2,6\text{-}Me_2C_6H_3O)]$ [e,h]	+2	-	32.58	**1.19**	16.5	98.7	IGAXIA V1	15
	+2	-	23.34	**2.65**	**8.5**	81.9	IGAXIA V2	15
$[V(PNP)_2(2,6\text{-}Me_2C_6H_3O)]$ [f,h]	+2	-	21.46	3.43	**8.5**	78.3	IGAXOG	15
$[V(PNP)_2(2,6\text{-}Me_2C_6H_3O)]$ [g,h]	+2	-	19.84	4.10	**8.1**	75.0	IGAXUM	15

[a] n is the number of bidentate ligands. [b] Path deviations (Dev.) and distortion coordinates (Dist.) in %. [c] nacnac = [ArNC(CH$_3$)]$_2$CH, Ar = 2,6-^{i}Pr$_2$C$_6$H$_3$. [d] This compound is closer to a seesaw (shape measure = 0.70). [e] PNP = 2,5-bis(di^{t}butylphosphinomethyl)R$_2$-pyrrolide, R = H (tridentate ligand). [f] R = Me. [g] R = Ph. [h] Normalized shape measures are given for these compounds.[16]

References for Table S5

1) W.C.A. Wilisch, M.J. Scott, W.H. Armstrong, *Inorg. Chem.*, 1988, **27**, 4333.

2) M. Rost, H. Gorls, W. Imhof, W. Seidel, K. Thiele, *Z. Anorg. Allgem. Chem.*, 1998, **624**, 1994.

3) K.L. Fujdala, T.D. Tilley, *Chem. Mater.*, 2002, **14**, 1376.

4) A.S. Veige, L.M. Slaughter, E.B. Lobkovsky, P.T. Wolczanski, N. Matsunaga, S.A. Decker, T.R. Cundari, *Inorg. Chem.*, 2003, **42**, 6204.

5) Y. Do, E.D. Simhon, R.H. Holm, *J. Am. Chem. Soc.*, 1983, **105**, 6731.

6) M. Moore, S. Gambarotta, C. Bensimon, *Organometallics*, 1997, **16**, 1086.

7) O. Ojelere, *CSD Communication*, 2019.

8) D. J. Brauer, H. Burger, G. R. Liewald, J. Wilke, *J. Organomet. Chem.*, 1986, **310**, 317.

9) D. R. Manke, D. G. Nocera, *Inorg. Chem.*, 2003, **42**, 4431.

10) B.L. Tran, B. Pinter, A.J. Nichols, F.T. Konopka, R. Thompson, C.-H. Chen, J. Krzystek, A. Ozarowski, J. Telser, M.-H. Baik, K. Meyer, D.J. Mindiola, *J. Am. Chem. Soc.*, 2012, **134**, 13035.

11) J. Cirera, E. Ruiz, S. Alvarez, *Inorg. Chem.*, 2008, **47**, 2871.

12) R. K. Minhas, J. J. H. Edema, S. Gambarotta, A. Meetsma, *J. Am. Chem. Soc.*, 1993, **115**, 6710.

13) A. F. Cozzolino, J. S. Silvia, N. López, C. C. Cummins, *Dalton Trans.*, 2014, **43**, 4639.

14) M.J. Scott, W.C.A. Wilisch, W.H. Armstrong, *J. Am. Chem. Soc.*, 1990, **112**, 2429.

15) Y. Sekiguchi, K. Arashiba, H. Tanaka, A. Eizawa, K. Nakajima, K. Yoshizawa, and Y. Nishibayashi, *Angew. Chem*., 2018, **130**, 9202.

16) S. Alvarez, B. Menjón, A. Falceto, D. Casanova, P. Alemany, *Inorg. Chem.*, 2014, **53**, 12151.

12 - References

[1] Inorg. Synth. **21**, 135 (1982)
[2] J. Am. Chem. Soc. **112**, 2429 (1990)
[3] J. Am. Chem. Soc. **120**, 4041 (1998)
[4] J. Magn. Res. **178**, 42 (2006)
[5] J. Chem. Phys. **102**, 4931 (1995); https://doi.org/10.1063/1.469541
[6] J. Chem. Phys. 115, 9113 (2001); https://doi.org/10.1063/1.1413524
[7] J. Phys. Chem. A **107**, 1872 (2003)
[8] Neese, F. "The ORCA program system" *Wiley interdisciplinary Reviews - Computational Molecular Science*, **2012**, Vol 2., Issue 1, Pages 73-78
[9] Chem. Phys. **356**, 98 (2009), https://doi.org/10.1016/j.chemphys.2008.10.036
[10] Bruker SMART V4.031. Program for Bruker CCD X-ray diffractometer control.; Bruker Analytical X-ray Systems Inc., Madison, WI, U.S.A., 1994.
[11] Bruker SAINT V4.028. Program for reduction of data collected on Bruker CCD Area detector diffractometers. Integration Software; Bruker Analytical X-ray Systems Inc., Madison, WI, U.S.A., 1994-6.
[12] Sheldrick, G. M. SHELXTL Program Package; Release 5.03; Bruker Analytical X-ray Systems Inc., Madison, WI, U.S.A., 1995.